Electronic Supplementary Material (ESI) for Journal of Materials Chemistry A.
This journal is © The Royal Society of Chemistry 2023

Supporting Information

Fabrication of Mesoporous Nickel Pyrophosphate Electrodes and Their Transformation to Nickel Hydroxide with Decent Capacitance in Alkali Media

Işıl Ulu,[1] Burak Ulgut,[1] Ömer Dag[1,2]*

[1]Department of Chemistry, Bilkent University, 06800, Ankara, Türkiye.
[2]UNAM — National Nanotechnology Research Center and Institute of Materials Science and Nanotechnology, Bilkent University, 06800, Ankara, Türkiye.

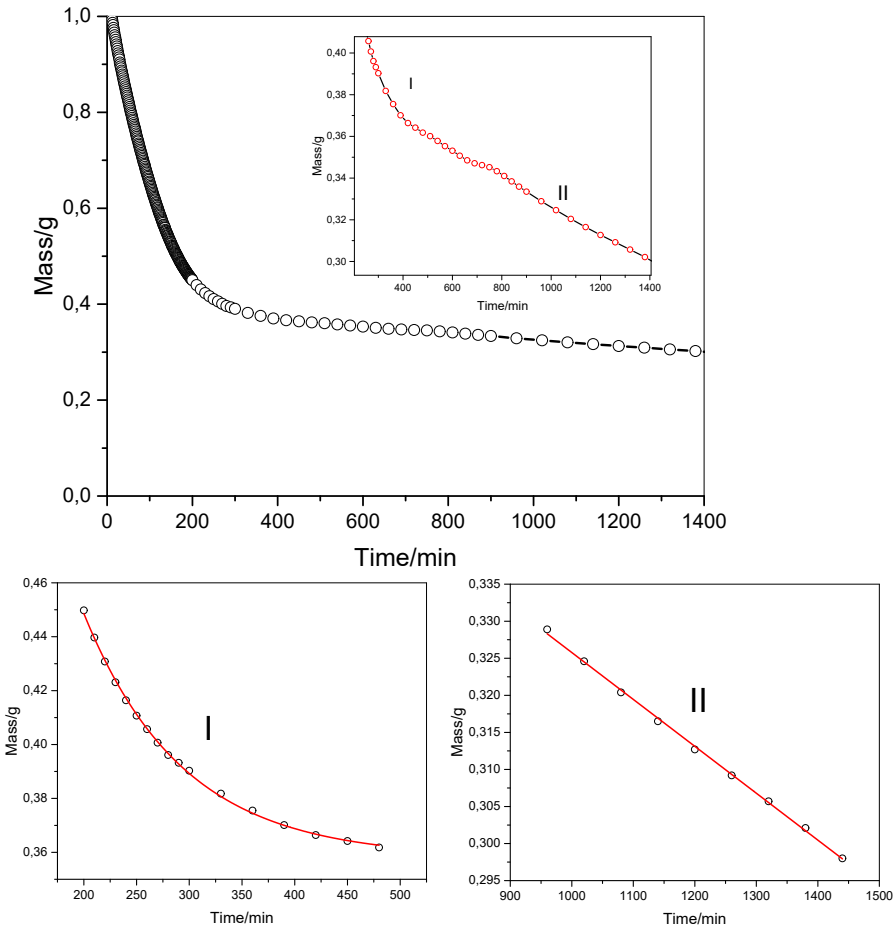

Fig. S1. Gravimetric measurements: Mass versus time plots during water evaporation on the balance of solution B.

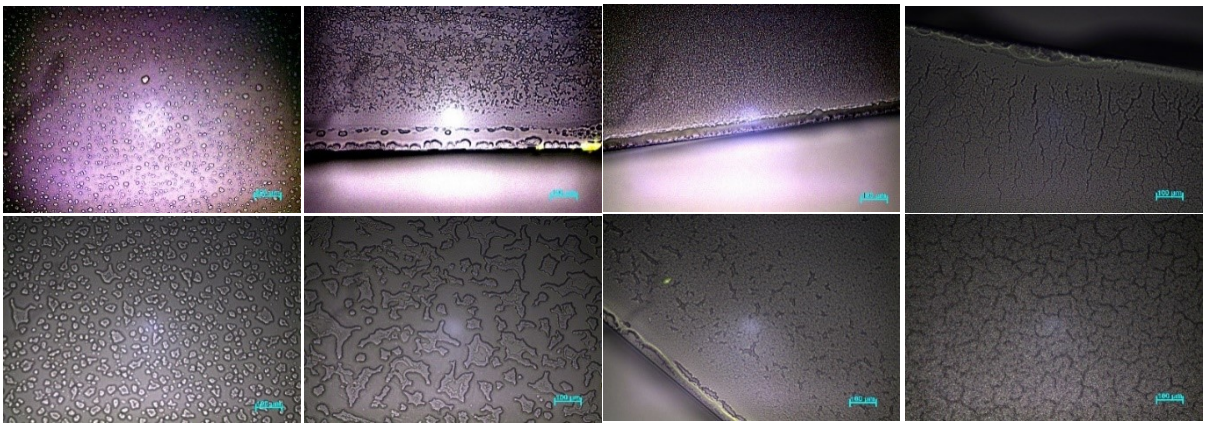

Fig. S2. POM images of (a, e) 10:5:1, (b, f) 20:10:1, (c, g) 40:20:1, and (d, h) 80:40:1 Ni(II):PPA:P123 after 15 min (top row) and 1 day (bottom row) aging/water evaporation (all scale bar are 100 µm).

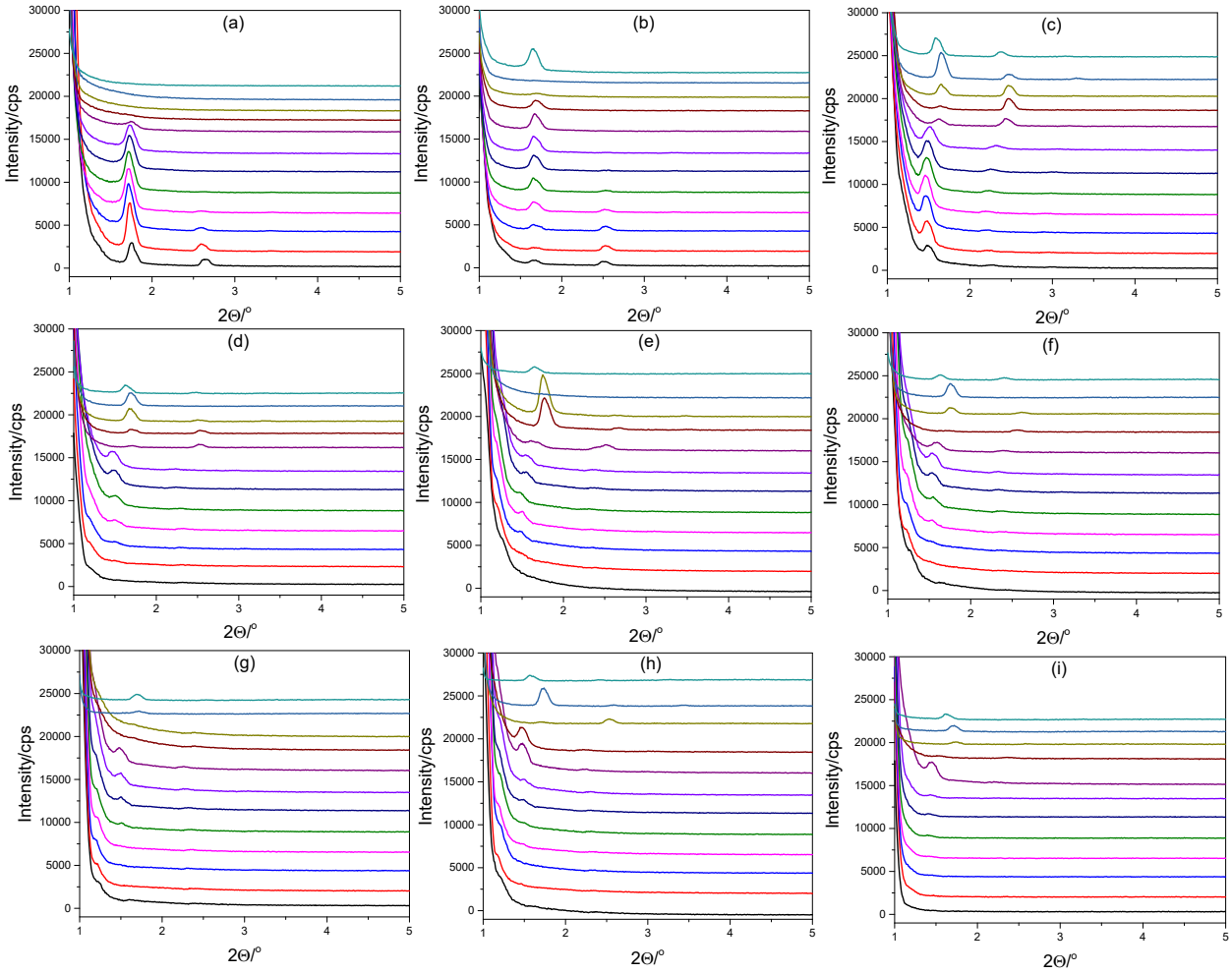

Fig. S3. Aging time-dependent (top to bottom, fresh, 10, 20, 30, 40, 50, 60, 90 min, 2, 3, 5, and 24 h) small-angle XRD pattern of Ni(II):PPA:P123 mole ratios of (a) 10:5:1, (b) 20:10:1, (c) 40:20:1, (d) 50:25:1, (e) 60:30:1, (f) 70:35:1, (g) 80:40:1, (h) 90:45:1, and (i) 100:50:1.

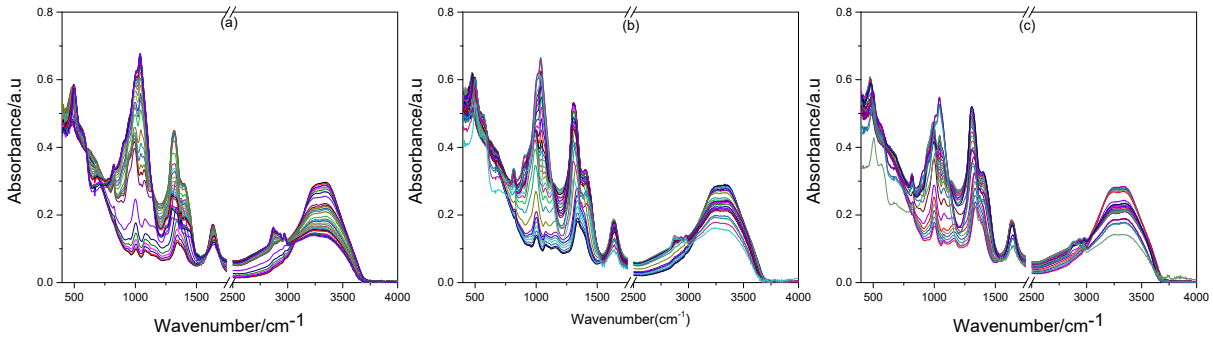

Fig. S4. The raw ATR-FTIR spectra of (a) solution A, (b) solution B, and (c) solution C (fresh, 5, 10, 15, 20, 25, 30, 40, 50, 60, 80, 100 min, 2, 2.5, 3, 3.5, 4, 5, 6, 7, 8, 9, 10, 11, 12, 19, 20, 22, 24, and 48 h aging).

ATR-FTIR Analysis:

The working principle of ATR-FTIR spectroscopy is based on a total internal reflection process. The internal infrared beam coming to the ATR crystal at a certain angle generates evanescent waves which extend throughout the sample; see Figure S5 (a) for the illustration. The penetration depth (d_p), which is a measure of how far the evanescent waves extend into the sample, can be calculated by the following equation[1]:

$$d_p = \frac{\lambda}{2\pi n_c \sqrt{sin^2\theta - (\frac{n_s}{n_c})^2}} \quad \text{eq. 1.}$$

where n_c and n_s are refractive indexes of the ATR crystal and the measured sample, respectively, λ is the wavelength of the IR beam and θ is the angle of the incident beam. The penetration depth depends on the refractive index of the sample and the wavelength of the coming IR beam. The wavelength dependence is handled by the spectrometer. The penetration depth dependence on the refractive index of the sample for each wavelength and a given wavelength are shown in Figure S5 (b) and (c), respectively. Since the thickness of the measured sample change during the water evaporation due to an increase in the refractive index of the sample, this change needs to be compensated for being able to compare the spectra with each other by normalization.

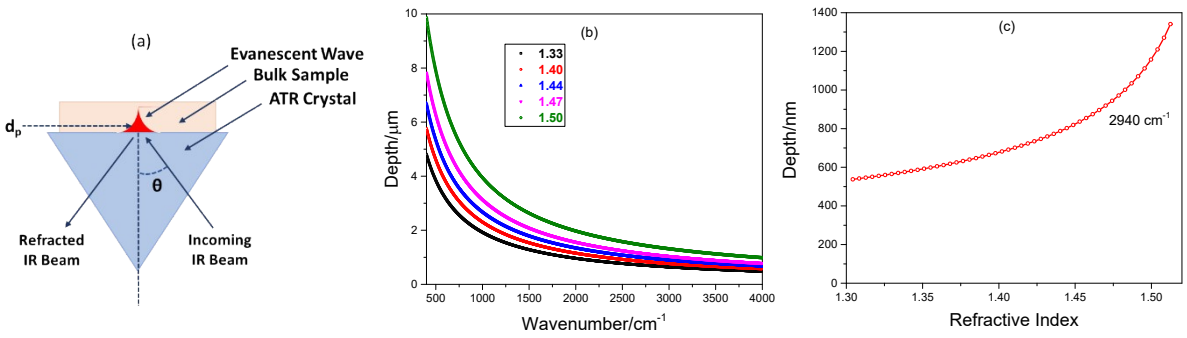

Fig. S5. (a) Schematic representation of evanescent wave resulting from the total reflection of ATR cell, (b) the depth versus wavenumber plots for various refractive indexes using equation 1, and (c) the depth versus refractive index for a specific wavenumber (2940 cm^{-1}).

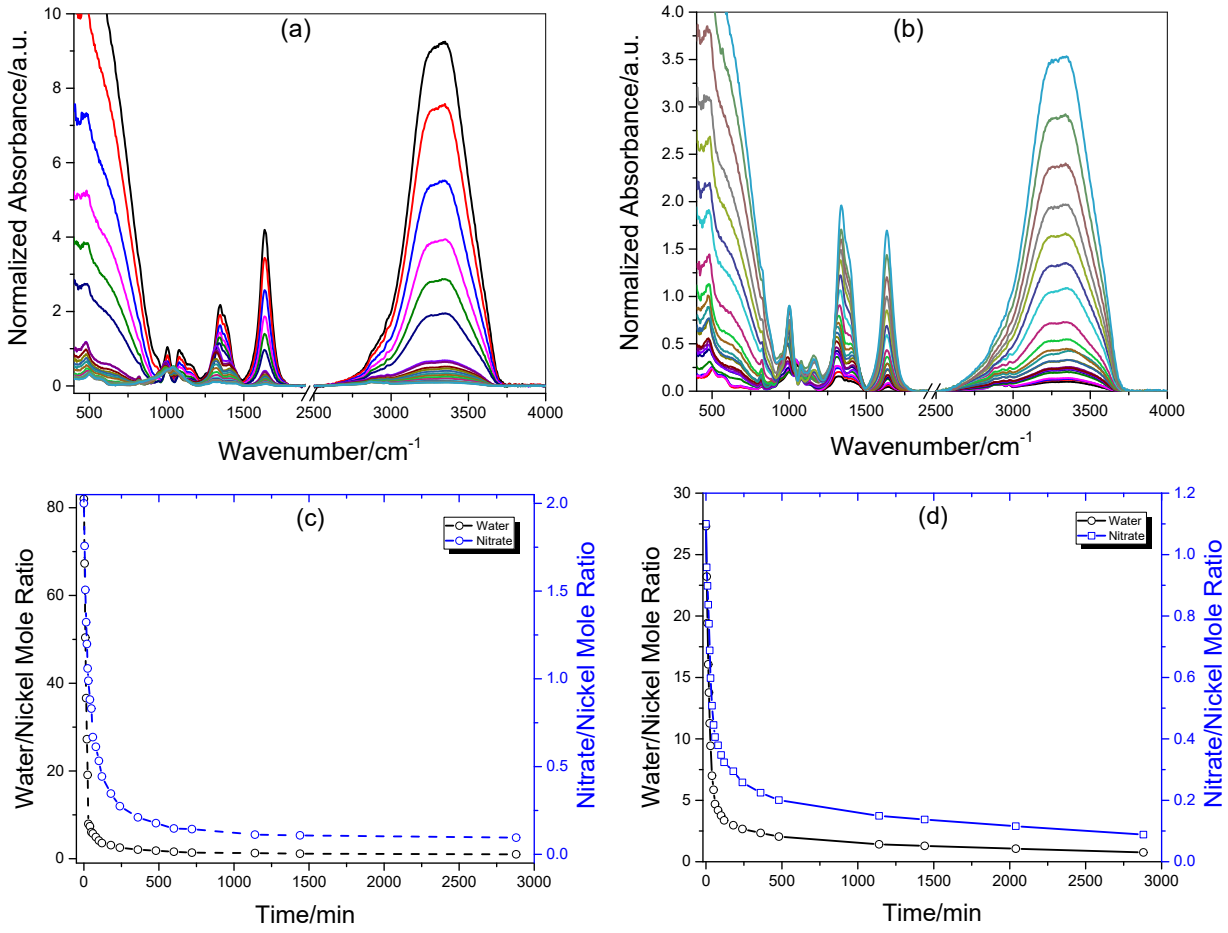

Fig. S6. Normalized ATR-FTIR spectra of (a) solution A, (b) solution C (top to bottom, fresh, 5, 10, 15, 20, 25, 30, 40, 50, 60, 80, 100 min, 2, 3, 4, 6, 8, 10, 12, 19, and 48 h aging), nitrate/nickel versus water/nickel mole ratio plots of (c) solution A, (d) solution C.

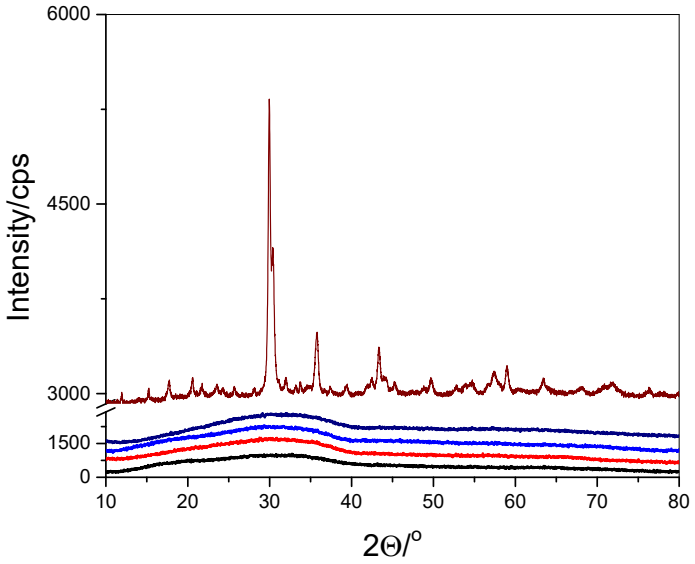

Fig. S7. XRD patterns of *m*-NiPP-60-X (X is 300, 400, 500, 600, and 700 °C from bottom to top.

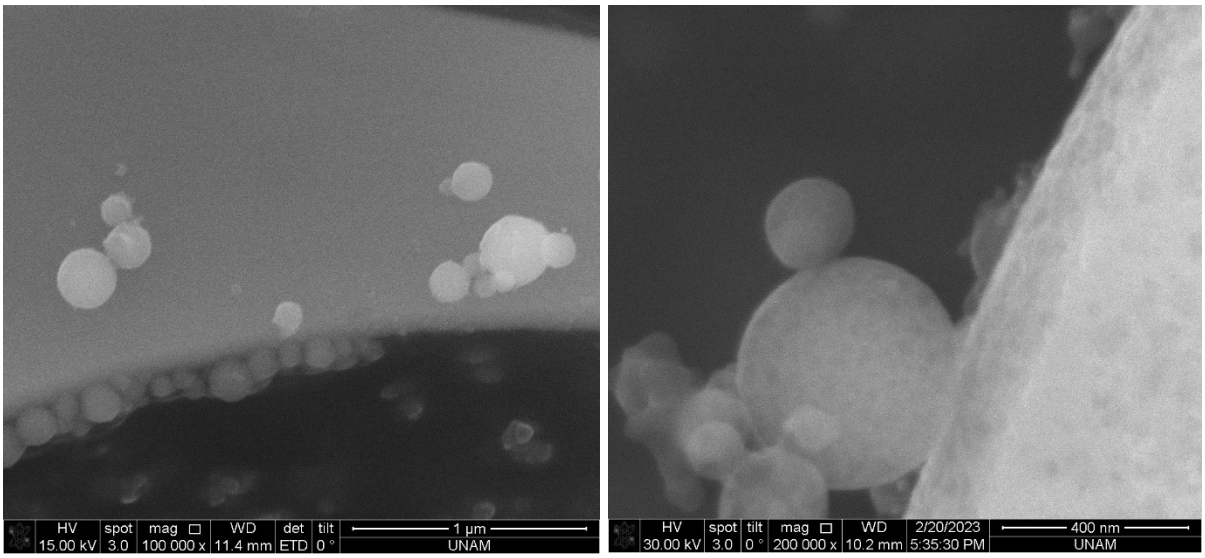

Fig. S8. SEM images of *m*-NiPP-60-X, X is (left) 300, (right) 600.

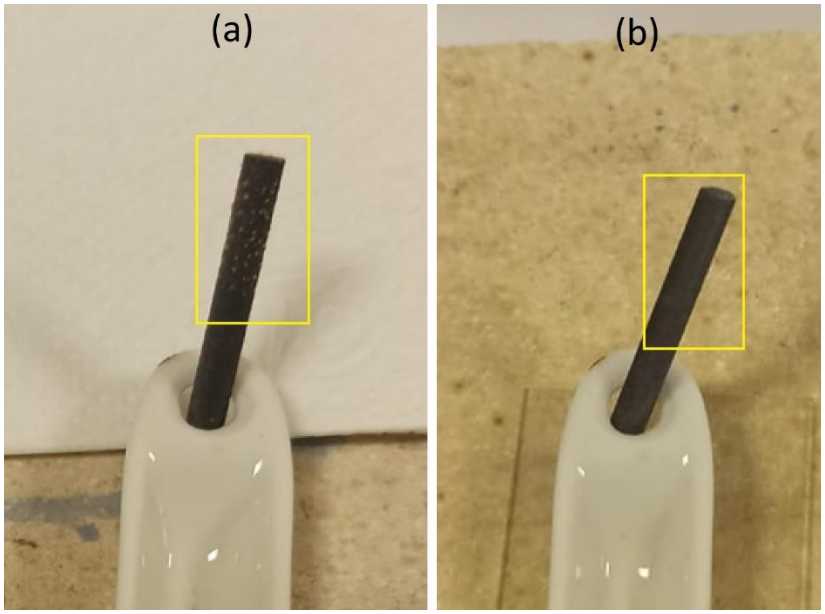

Fig. S9. Photographs of the GR-NiPP electrodes, (a) dip-coated from mother liquid of solution A and (b) 5 times diluted solution from solution A and calcined at 300 °C, yellow rectangle parts are coated.

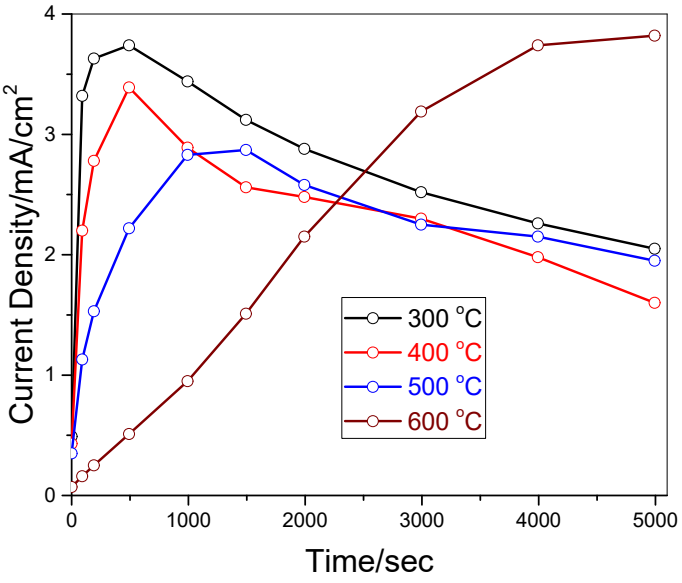

Fig. S10. Current density versus time plots of FTO-NiPP-60-X (X is 300, 400, 500, and 600) derived from m-CVs by taking the current densities of reduction peak maxima.

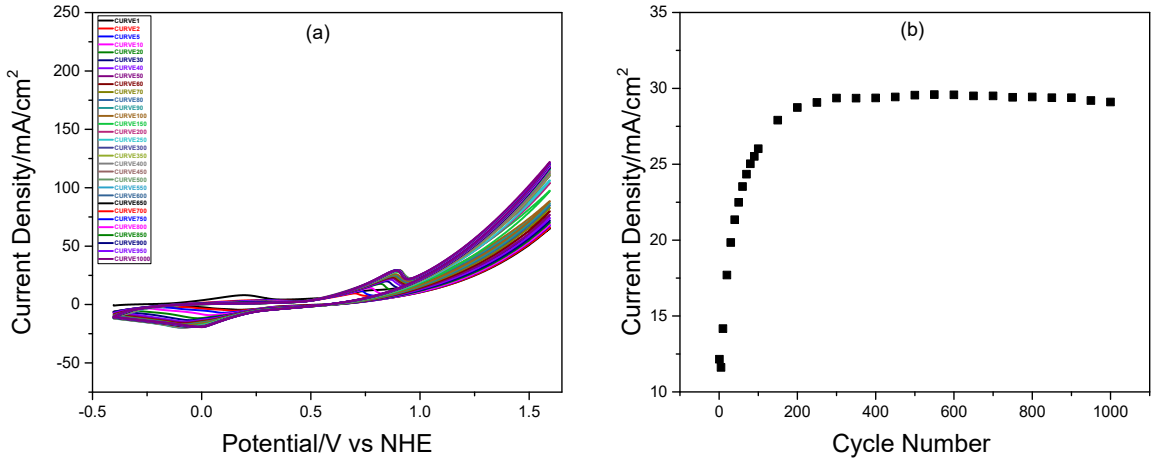

Fig. S11. (a) m-CV cycles of GR-NiPP-30-700 electrode with the scan rate of 50 mV/s, (b) current density versus cycle number plot of GR-NiPP-30-700 derived from m-CVs by taking the current densities of oxidation peak maxima for 1000 cycles.

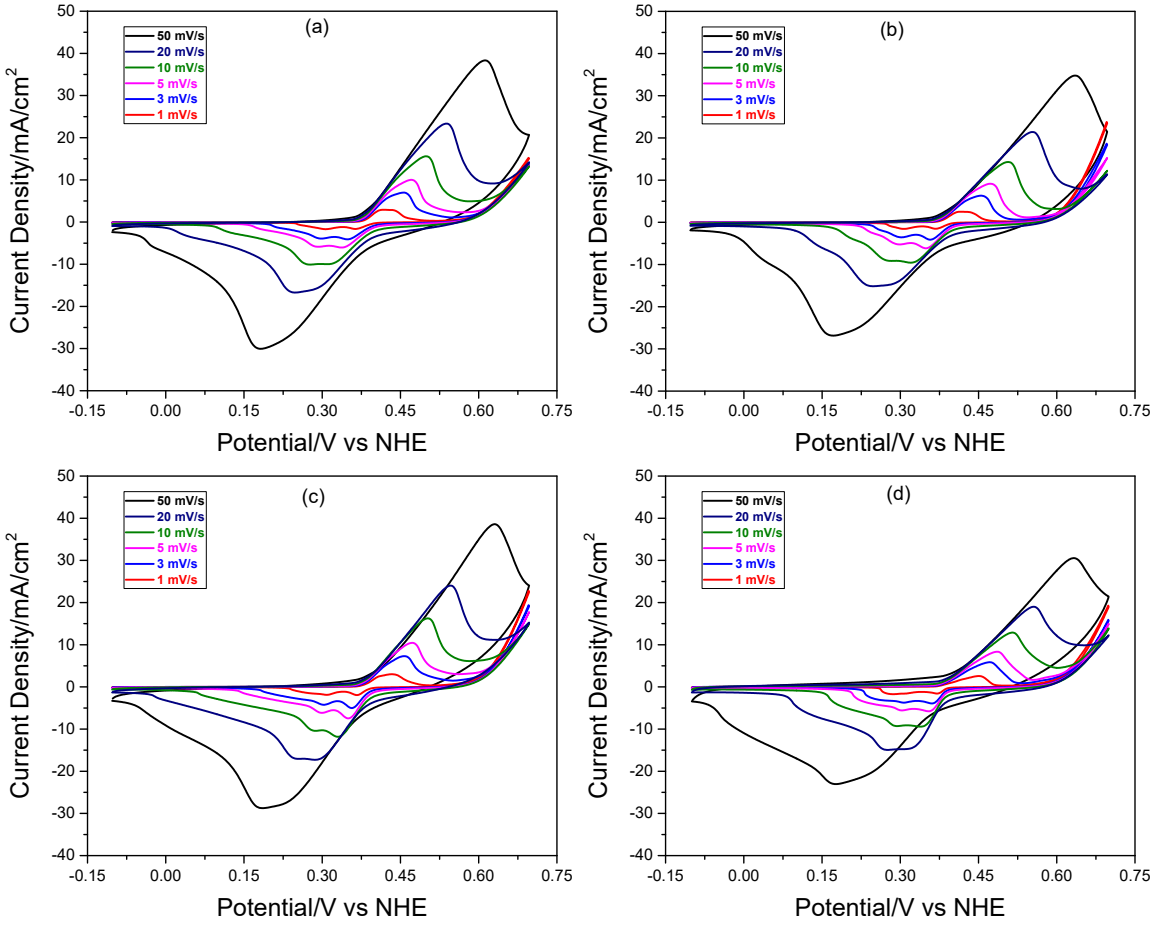

Fig. S12. Scan rate-dependent CVs of GR-NiPP-30-X (X is (a) 400, (b) 500, (c) 600, and (d) 700 ^{o}C).

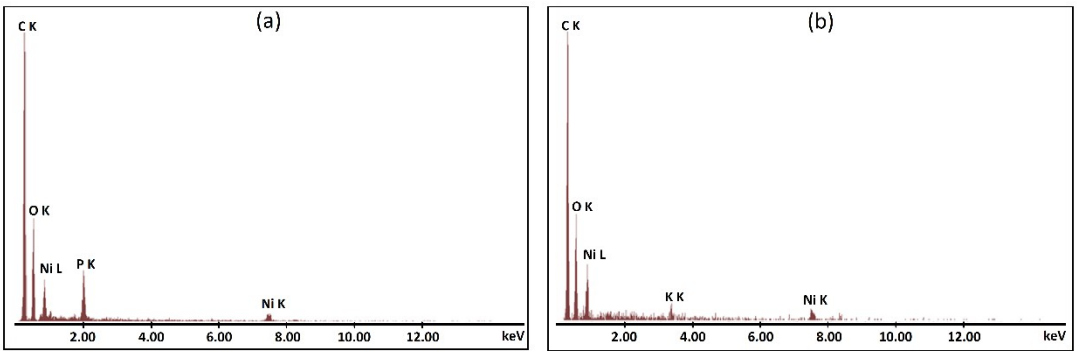

Fig. S13. EDX spectra of *m*-NiPP-30-300 (a) before and (b) after m-CV measurements.

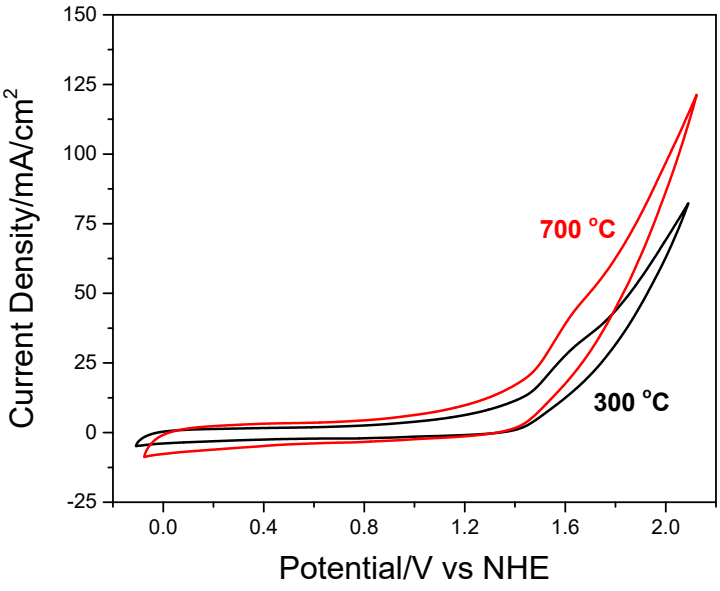

Fig. S14. The 50th cycle CV curves of GR-NiPP-30-X (300 and 700 ^{o}C) in an electrolyte consisting of 2.4 M KOH and 0.6 PPA with a scan rate of 50 mV/s.

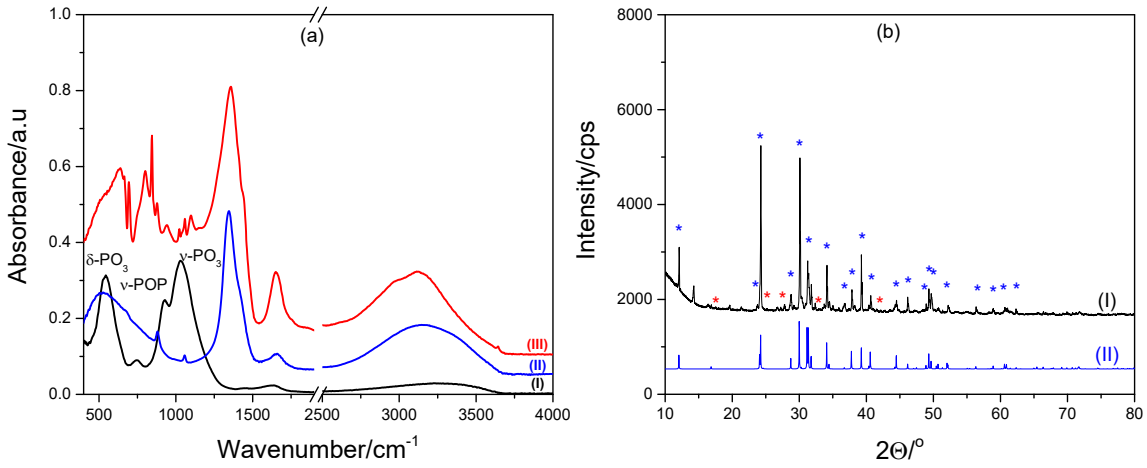

Fig. S15. (a) ATR-FTIR spectra of (I) NiPP-60-300, (II) dried KOH solution for 1 h at ambient conditions, and (III) aged NiPP-60-300 sample on the microscope slide in 3M KOH solution for 1 h, (b) wide angle XRD patterns of (I) aged NiPP-60-300 sample on the microscope slide in 3M KOH solution for 1 h indexed with (II) $KHCO_3$ (ICDD 01-082-1447) database (showed by blue stars) and minimal amount of KOH (ICDD 00-021-0645) database (showed by red stars).

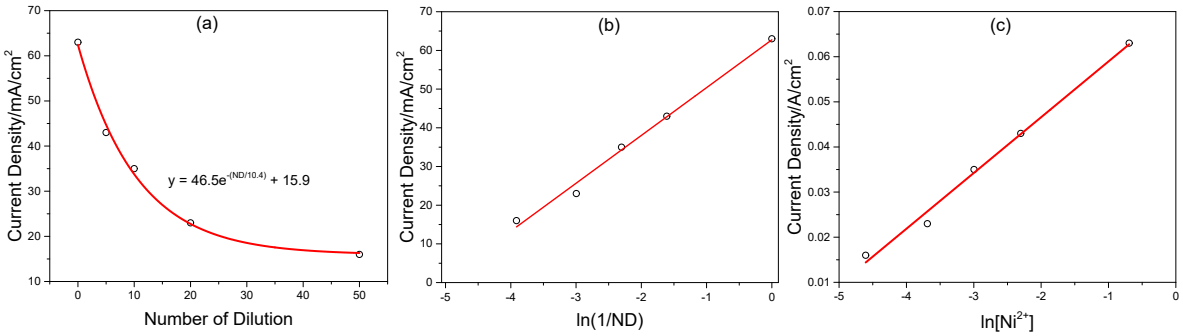

Fig. S16. (a) Current density versus the number of dilution plot, (b) current density versus ln(1/ND) plot, and (c) current density versus ln[Ni^{2+}] plot of GR-NiPP-30-300 electrode.

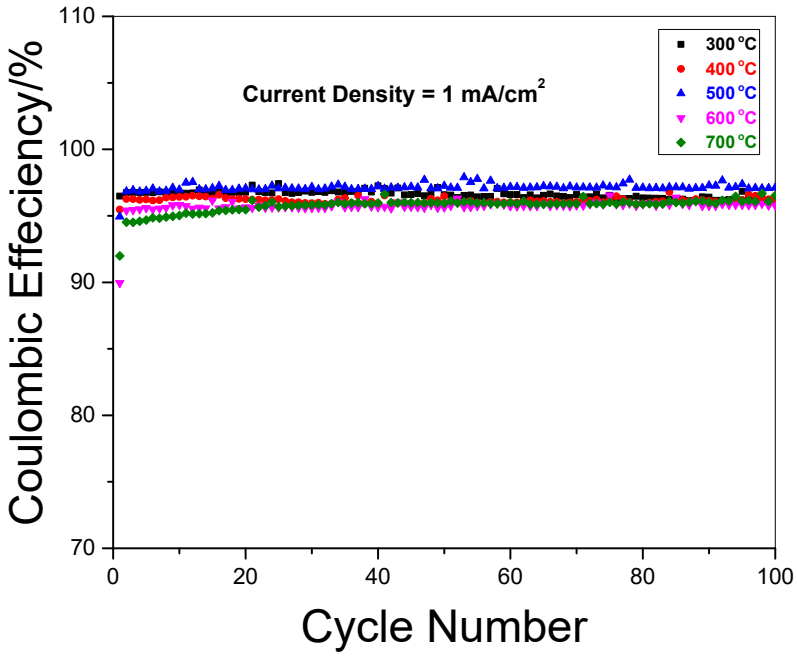

Fig. S17. The coulombic efficiency versus number of GCD cycles plot of the GR-NiPP-X electrodes (X is 300, 400, 500, 600, and 700).

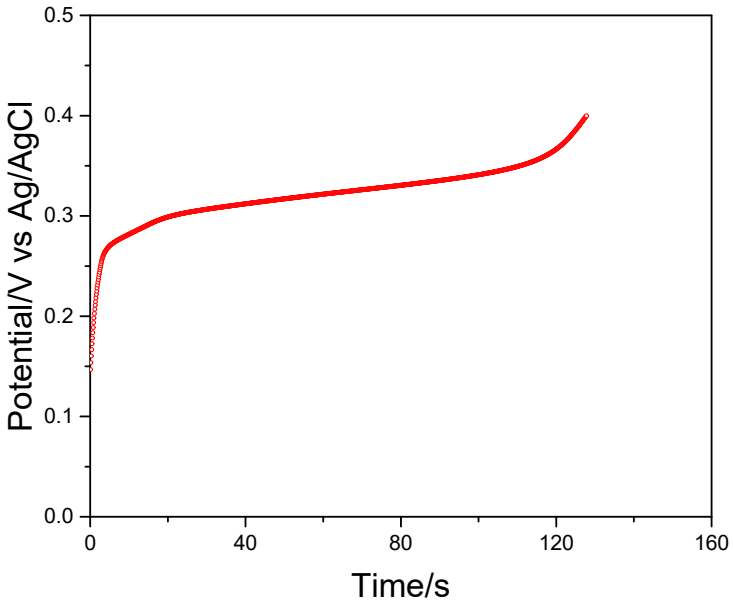

Fig. S18. The raw galvanostatic charge data of GR-NiPP-60-700 sample at 1 mA/cm^2 current density.

Fig. S18 shows the raw data of galvanostatic charging feature of GR-NiPP-60-700 sample at 1 mA/cm^2 current density. Even though the potential window for charging is adjusted as 0.1-0.4 V, the first point recorded during charging is more positive than 0.1 V (it is around 0.15 V). This is also valid for discharging value, which is starting from a value negative of 0.4 V. These differences are due to effects that are hard to control such as the series resistance, the time between the applied current and the first point recorded and the state of the electrode after the end of the previous discharge. When calculating a capacitance, the software is using the first and the last points in potential. Since the system is more Faradaic than capacitive, comparing the capacity values of materials is more reliable. We are only reporting capacitance values in order to report a number that is comparable to published values. We are well aware that the capacitance number can be increased simply by using a smaller potential window that includes the bulk of the charge.

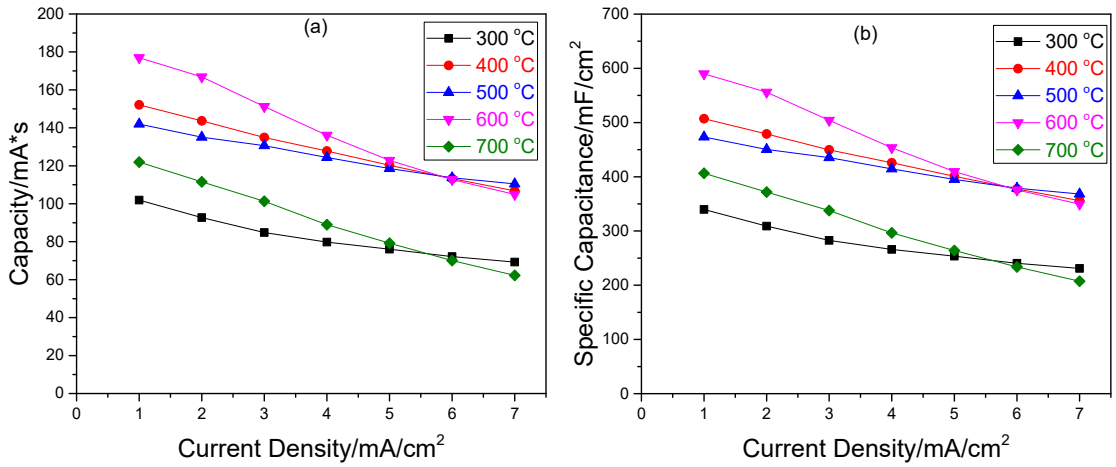

Fig. S19. (a) Capacity, (b) specific capacitance versus current density plots of GR-NiPP-30-X (X is 300, 400, 500, 600, and 700) electrodes.

Table S1. Amounts of ingredients used for the solutions of given molar ratios for NiPP.

Mole ratio of the ingredients	P123 (g)	$H_4P_2O_7$ (g)	$[Ni(H_2O)_6](NO_3)_2$ (g)
1:10:5	1.000	0.155	0.506
1:20:10	1.000	0.310	1.011
1:30:15	1.000	0.465	1.517
1:40:20	1.000	0.620	2.022
1:50:25	1.000	0.775	2.529
1:60:30	1.000	0.929	3.034
1:70:35	1.000	1.084	3.540
1:80:40	1.000	1.239	4.046
1:90:45	1.000	1.393	4.552
1:100:50	1.000	1.548	5.057

References

1 B. C. Smith, *Fundamentals of Fourier Transform Infrared Spectroscopy*; CRC Press, 2011.